First publ. in: Applied physics letters 93 (2008), 8, No. 3512

Fully epitaxial Fe(110)/MgO(111)/Fe(110) magnetic tunnel junctions: Growth, transport, and spin filtering properties

J. O. Hauch,[1] M. Fonin,[2,a)] M. Fraune,[1] P. Turban,[3] R. Guerrero,[4] F. G. Aliev,[4] J. Mayer,[5] U. Rüdiger,[2] and G. Güntherodt[1]
[1]*II. Physikalisches Institut, RWTH Aachen University, 52056 Aachen, Germany*
[2]*Fachbereich Physik, Universität Konstanz, 78457 Konstanz, Germany*
[3]*Equipe de Physique des Surfaces et Interfaces, Institut de Physique de Rennes, CNRS UMR 6251, Université de Rennes, Campus de Beaulieu, Bâtiment 11 C, 35042 Rennes Cedex, France*
[4]*Departamento de Fisica de la Materia, C-III, Universidad Autónoma de Madrid, Cantoblanco, 28049 Madrid, Spain*
[5]*Gemeinschaftslabor für Elektronenmikroskopie, RWTH Aachen University, 52056 Aachen, Germany*

Fully epitaxial Fe(110)/MgO(111)/Fe(110) magnetic tunnel junctions (MTJs) have been tested with respect to symmetry-enforced spin filtering. The Fe(110) electrodes exhibit $\Sigma_{1\uparrow}$ and $\Sigma_{1\downarrow}$ spin states, both crossing the Fermi level, but with a group velocity about 50% smaller for the minority states compared to the majority ones. These epitaxial but symmetry-mismatched MTJs yield tunneling magnetoresistance (TMR) values of 54% at 1.5 K and 28% at room temperature. The TMR value and the estimated tunneling spin polarization are consistent with a partial spin filtering due to the $\Sigma_{1\uparrow}$ states partially compensated by the $\Sigma_{1\downarrow}$ states. © *2008 American Institute of Physics*.

In recent years magnetic tunnel junctions[1,2] (MTJs) have attracted increasing attention because of their potential applications in spintronic devices. The potential of the epitaxial Fe(100)/MgO(100)/Fe(100) system has been emphasized by its theoretically predicted extremely high tunneling magnetoresistance (TMR) values exceeding 1000%.[3] Intense efforts have been focused on the fabrication of junctions with large TMR values at room temperature (RT),[4–11] reaching record values of 410% using bcc Co[10] and of 500% using nominally amorphous CoFeB.[11] For fully epitaxial Fe(100)/MgO(100)/Fe(100) MTJs prepared by molecular beam epitaxy (MBE) maximum TMR values of 180%[6] have been obtained at RT.

The crucial feature of these MTJs is the conservation of spin and symmetry of the tunneling electrons. This is fulfilled most ideally for the majority electron spins of Δ_1 symmetry tunneling along the [100] direction of MgO-based MTJs.[4–7,10] In turn, manifold tests of the symmetry-enforced high spin-polarized tunneling current in fully epitaxial or highly textured MTJs have been undertaken using diverse ferromagnetic (FM) electrodes and MgO barriers. For example, the use of metallic nonmagnetic or FM spacer layers at the FM/MgO interface resulted in spin filtering due to spin-polarized quantum well states[12,13] or due to spin-symmetry gaps.[14] On the other hand, interfaces with a symmetry mismatch have been found to yield symmetry-dependent filtering for tunneling electron spins at energies high enough to overcome the tunnel barrier.[15]

In this work we study the spin filtering in fully epitaxial Fe(110)/MgO(111)/Fe(110) MTJs with the dense but grainy MgO layer. Epitaxially grown (110)-oriented bcc Fe layers are advantageous because of a large in-plane uniaxial magnetocrystalline anisotropy, which yields well defined switching states of the magnetization.[16] Moreover, they exhibit a high spin polarization value of about −80% measured near the Fermi energy (E_F) using spin- and angle-resolved photoelectron spectroscopy (SP-ARPES) with $h\nu$=21.2 eV.[17] This photoemission-derived spin polarization originates dominantly from less dispersing $\Sigma_{1\downarrow}$ states close to the Γ point and slightly below E_F (see Fig. 1).[17–19] For the spin-polarized tunneling, however, the $\Sigma_{1\downarrow}$ and $\Sigma_{1\uparrow}$ spin states along the [110] direction of Fe, both crossing E_F near the N point of the Brillouin zone[18,19] (see Fig. 1), may be of relevance because of their large spatial extent. This special situation allows for a twofold test of (i) the symmetry-dependent spin filtering effect of s-like tunnel electron states[3] and (ii) the distinction between the spin-polarized states contributing to photoemission and to tunneling. For our fully epitaxial Fe(110)/MgO(111)/Fe(110) MTJs we obtain TMR values of 54% at 1.5 K and 28% at RT. This evidences a reduced spin filtering by the $\Sigma_{1\uparrow}$ spin states at E_F near the N point, which are partially compensated by the $\Sigma_{1\downarrow}$ states crossing E_F

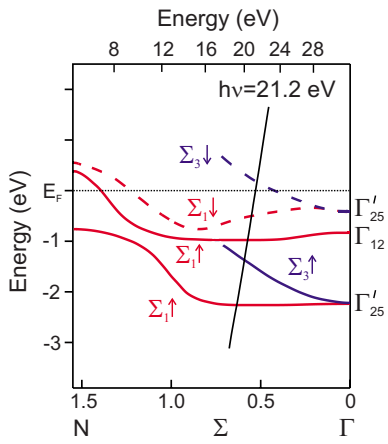

FIG. 1. (Color online) Schematic spin-split band structure of Fe along the [110], Γ-Σ-N direction adapted according to Refs. 18 and 19; spin-up (-down) states: solid (dashed) lines. The free electron final band is shifted by E=21.2 eV with its energy displayed along the top scale.

a)Author to whom correspondence should be addressed. Electronic mail: mikhail.fonin@uni-konstanz.de.

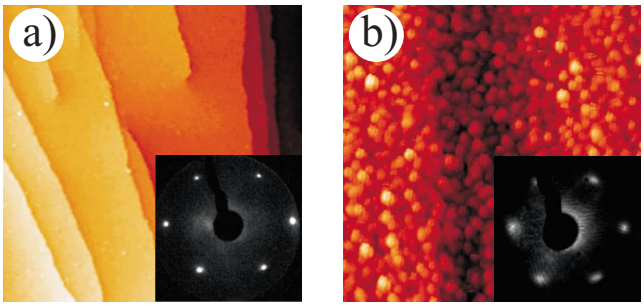

FIG. 2. (Color online) (a) STM image (100×100 nm^2) of a 25 nm thick Fe(110) film on Mo(110)/$Al_2O_3(11\bar{2}0)$ (1.0 V; 0.12 nA). The inset shows the corresponding LEED image (E_{beam}=90 eV). (b) STM image (100×100 nm^2) of a 1 nm thick MgO layer deposited on Fe(110) (3.6 V; 0.35 nA). The inset shows the LEED image of a 3 nm thick MgO layer (E_{beam}=101 eV).

nearby, but with about a 50% smaller group velocity.

All epitaxial Fe/MgO/Fe MTJs were grown by MBE under ultrahigh vacuum conditions. A 25 nm thick Fe(110) layer (bottom electrode) was deposited on Mo(110)/$Al_2O_3(11\bar{2}0)$ at RT and subsequently annealed at 640 K. MgO layers were deposited directly from bulk MgO by electron beam evaporation onto the Fe(110) layer kept at RT. As magnetic top electrode a 10 nm thick epitaxial Fe(110) film was deposited at RT. All samples were covered by a 5 nm thick Au cap layer to prevent oxidation during *ex situ* handling and measurements. The multilayer structure was patterned using a combination of optical and electron beam lithography and Ar^+ ion milling. All transport measurements were performed on epitaxial MTJs of two different sizes (10×10 μm^2 and 20×20 μm^2) using an ac four point method.

Figure 2(a) shows a scanning tunneling microscopy (STM) image of the atomically flat Fe(110) surface of the bottom electrode. The (1×1) low-energy electron diffraction (LEED) pattern of twofold symmetry [inset in Fig. 2(a)], typical for the bcc Fe(110) surface, confirms its high quality. The surface morphology of a 1 nm thick MgO film deposited at RT on Fe(110) is shown in Fig. 2(b). The MgO grains visible in the STM image give clear evidence of a three-dimensional growth mode of MgO. After the deposition of 3 nm of MgO a well-ordered hexagonal (1×1) LEED pattern corresponding to MgO(111) was observed [inset of Fig. 2(b)]. Because of the grainy structure the MgO barrier thickness for all MTJs has been chosen rather thick, i.e., nominally 4 nm. A 10 nm thick epitaxial Fe(110) top electrode was deposited at RT onto the MgO layer. The epitaxial relationship of the MgO(111)/Fe(110) system as well as the growth of the Fe(110) top electrode were monitored using reflection high-energy electron diffraction (not shown).

A typical cross section transmission electron microscopy (TEM) image of the epitaxial MTJ is shown in Fig. 3(a). The interfaces between the different layers are clearly discernible as abrupt and without any indication of interdiffusion. The MgO barrier shows no indication of defects (pinholes) in spite of the three-dimensional growth mode on Fe(110). Thus the MgO layer is a dense, though grainy insulating barrier. Figure 3(b) shows a typical hysteresis loop of the epitaxial MTJ with the magnetic field applied parallel to the [001] in-plane direction (magnetic easy axis) of the Fe(110) electrodes. The switching of the first layer at approximately 65

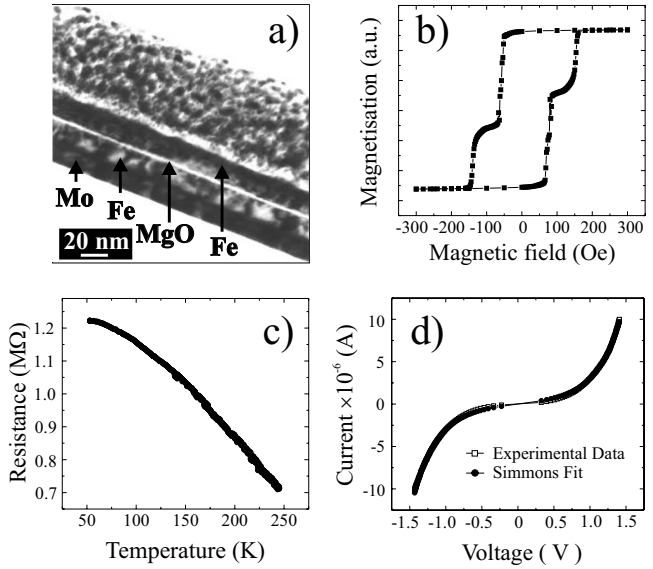

FIG. 3. (a) TEM micrograph of a cross section of the epitaxial Fe(110)/MgO(111)/Fe(110) MTJ. (b) Magnetic hysteresis loop at 4.2 K and (c) a typical $R(T)$ curve of the MTJ. (d) I-U characteristics of the Fe/MgO/Fe MTJ measured at 4.2 K (open squares) together with the corresponding Simmons fit[21] of the experimental data (full circles).

Oe already results in a reversal of the magnetization. Therefore, the thicker (bottom) electrode has the lower coercivity. The magnetic hard, thinner (top) electrode switches at approximately 145 Oe. A typical temperature dependence of the tunneling resistance $R(T)$ of the epitaxial MTJ is presented in Fig. 3(c). The tunneling resistance decreases from 1.2 MΩ at 4.2 K to 700 kΩ at 250 K, showing an insulatorlike behavior of the MTJ. This gives proof of a pinhole-free barrier.[20] The current-voltage (I-U) characteristics of the epitaxial MTJ measured at 4.2 K show a typical nonlinear dependence [see Fig. 3(d)]. The tunneling barrier height Θ and barrier width d estimated by a numerical fitting procedure using the Simmons model[21] are Θ=2.0 eV and d=1.5 nm, respectively. The estimated barrier width is significantly smaller than the nominal 4 nm thick MgO layer. We suggest that this has to do partly with the grainy structure of the MgO(111) layer allowing for some limited intrusion of Fe into the oxide layer, leading to an on average smaller than nominal MgO barrier thickness. An effectively reduced (about halved) barrier thickness may also be accounted for by resonant tunneling via localized states dominantly in the middle of the barrier.[22]

Figure 4 shows the TMR curves measured for a micro-

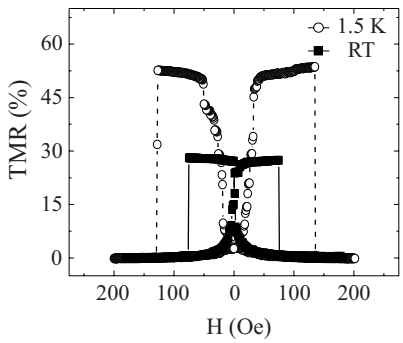

FIG. 4. TMR measurements as a function of external magnetic field at 1.5 K (open circles) and at RT (full squares).

structured MTJ (20×20 μm^2). The TMR is defined as $(R_{AP}\text{-}R_P)/R_P$ with tunneling resistances for antiparallel (R_{AP}) and parallel (R_P) magnetization directions. The epitaxial MTJ shows a TMR ratio of about 54% at 1.5 K, which drops gradually with increasing temperature, yielding about 28% at RT. On the basis of the simple Jullière model[23] we determined from the TMR value at 1.5 K a rough estimate of the absolute value of the tunneling spin polarization of the Fe(110) electrodes of about P_t=46.1%. This value is of the order of P_t=40% of polycrystalline Fe,[24] but way below P_t =74% of annealed, (100)-textured Fe, yielding 290% TMR at low temperature.[7] The magnitude of our 54% TMR points to a reduced spin filtering by the $\Sigma_{1\uparrow}$ spin states, crossing E_F nearest to the N point. The symmetry-dependent spin filtering by these states will be partially compensated by the $\Sigma_{1\downarrow}$ states, crossing E_F less close to the N point with a roughly 50% smaller group velocity. We argue that the $\Sigma_{1\uparrow}$ states at E_F and nearest to the N point have about half the density of states compared to the $\Sigma_{1\downarrow}$ states.[19] A crude estimate of the spin polarization due to the $\Sigma_{1\uparrow}$ and $\Sigma_{1\downarrow}$ states near E_F yields $|P_t|\cong33\%$ in reasonable agreement with P_t estimated by the Jullière model above.

On the other hand, under our experimental conditions of the SP-ARPES experiment[17] the allowed electronic states contributing to the photoemission spin polarization along the [110] direction may be of Σ_1, Σ_3, and Σ_4 symmetries,[18,25,26] as derived from the $\Gamma'_{25\downarrow}$ and $\Gamma_{12\uparrow}$ states. For $h\nu$=21.2 eV photon energy and an energy resolution of 100 meV a dominant contribution to the photoemission spin polarization near E_F arises from the $\Sigma_{1\downarrow}$ states closer to the zone center (see Fig. 1).[17,18] The latter account mainly for the −80% spin polarization in SP-ARPES, but do not play a role for the spin-polarized tunneling. A possible small contribution may be due to the $\Sigma_{3\downarrow}$ states,[18] which are crossing E_F close to the zone center (see Fig. 1). The latter, however, are less favored for tunneling because of their high angular momentum.[27]

Despite the fact that for Fe(110) both the $\Sigma_{1\downarrow}$ and $\Sigma_{1\uparrow}$ states are crossing E_F, there is a slight asymmetry in spin-polarized tunneling conductance because of some prevailing d-character of the minority states at E_F compared to the prevailing s-character of the majority states.[27] The tunneling from these states of Fe(110) with $k_\parallel\neq0$ may in principle be impeded by the 4 nm thick MgO barrier. However, an effectively smaller barrier thickness (see above) may alleviate this problem. However, tunneling through the MgO(111) barrier via its Λ_1 states[28] with (s,p,d)-character,[27,28] starting from symmetry-mismatched Σ_1 states of Fe(110), may present another obstacle. Hence the transmission probability or conductance of the majority electrons will be severely attenuated as compared to the case of the Fe(100)/MgO(100)/Fe(100) MTJs. The attenuation will be determined by the imaginary part of the wavevector along the [111]-direction of the complex band structure in the gap region of MgO. This may explain the rather small TMR values found in our work.

In conclusion, the (110) orientation of the Fe electrodes in epitaxially MBE grown Fe(110)/MgO(111)/Fe(110) MTJs appears as an intricate test case for TMR in terms of symmetry-enforced spin filtering of off-normal tunneling contributions. For the (110) orientation of Fe, the spin filtering effect in tunneling of Σ_1 majority spin electrons with s-character is partially compensated by the states of the same symmetry, crossing E_F for the minority channel. However, the roughly 50% smaller group velocity of the latter states favors the tunneling from $\Sigma_{1\uparrow}$ states. A reduced effective tunnel barrier thickness and resonant tunneling may enable the required off-normal tunneling. However, the (111) orientation of the MgO barrier with symmetry-mismatched Λ_1 states with s,p,d-character may severely attenuate the transmission probability compared to the (100) orientation. In this light the measured TMR values as high as 54% at 1.5 K (28% at RT) are somewhat unexpected. The difference in spin polarization in tunneling and SP-ARPES has been identified as due to, respectively, near-zone-boundary s-type $\Sigma_{1\uparrow}$ states at E_F, partly compensated by d-like $\Sigma_{1\downarrow}$ states, and due to mainly near-zone-center $\Sigma_{1\downarrow}$ states slightly below E_F.

This work was supported by BMBF, Grant No. FKZ 13N7329. Work in Madrid was supported by Spanish MEC (MAT2006-07196). The authors would like to thank A. Bückins for the help with the TEM measurements.

[1]T. Miyazaki and N. Tezuka, J. Magn. Magn. Mater. **139**, L231 (1995).
[2]J. S. Moodera, L. R. Kinder, T. M. Wong, and R. Merservey, Phys. Rev. Lett. **74**, 3273 (1995).
[3]W. H. Butler, X. G. Zhang, T. C. Schulthess, and J. M. MacLaren, Phys. Rev. B **63**, 054416 (2001).
[4]M. Bowen, V. Cros, F. Petroff, A. Fert, C. Martinez Boubeta, J. L. Costa-Krämer, J. V. Anguita, A. Cebollada, F. Briones, J. M. de Teresa, L. Morelln, M. R. Ibarra, F. Gell, F. Peir, and A. Cornet, Appl. Phys. Lett. **79**, 1655 (2001).
[5]F. Faure-Vincent, C. Tiusan, E. Jouguelet, F. Canet, M. Sajieddine, C. Bellouard, E. Popova, M. Hehn, F. Montaigne, and A. Schuhl, Appl. Phys. Lett. **82**, 4507 (2003).
[6]S. Yuasa, T. Nagahama, A. Fukushima, Y. Suzuki, and K. Ando, Nat. Mater. **3**, 868 (2004).
[7]S. S. P. Parkin, C. Kaiser, A. Panchula, P. M. Rice, B. Hughes, M. Samant, and S. H. Yang, Nat. Mater. **3**, 862 (2004).
[8]D. D. Djayaprawira, K. Tsunekawa, M. Nagai, H. Maehara, S. Yamagata, N. Watanabe, S. Yuasa, Y. Suzuki, and K. Ando, Appl. Phys. Lett. **86**, 092502 (2005).
[9]Y. M. Lee, J. Hayakawa, S. Ikeda, F. Matsukura, and H. Ohno, Appl. Phys. Lett. **89**, 042506 (2006).
[10]S. Yuasa, A. Fukushima, H. Kubota, Y. Suzuki, and K. Ando, Appl. Phys. Lett. **89**, 042505 (2006).
[11]Y. M. Lee, J. Hayakawa, S. Ikeda, F. Matsukura, and H. Ohno, Appl. Phys. Lett. **90**, 212507 (2007).
[12]T. Nagahama, S. Yuasa, Y. Suzuki, and E. Tamura, Appl. Phys. Lett. **79**, 4381 (2001).
[13]S. Yuasa, T. Nagahama, and Y. Suzuki, Science **297**, 234 (2002).
[14]F. Greullet, C. Tiusan, F. Montaigne, M. Hehn, D. Halley, O. Bengone, M. Bowen, and W. Weber, Phys. Rev. Lett. **99**, 187202 (2007).
[15]M. Bowen, A. Barthélémy, V. Bellini, M. Bibes, P. Seneor, E. Jacquet, J.-P. Contour, and P. H. Dederichs, Phys. Rev. B **73**, 140408 (2006).
[16]J. Yu, U. Rüdiger, A. D. Kent, L. Thomas, and S. S. P. Parkin, Phys. Rev. B **60**, 7352 (1999).
[17]Yu. S. Dedkov, U. Rüdiger, and G. Güntherodt, Phys. Rev. B **65**, 064417 (2002); R. Kurzawa, K.-P. Kämper, W. Schmitt, and G. Güntherodt, Solid State Commun. **60**, 777 (1986).
[18]A. M. Turner and J. L. Erskine, Phys. Rev. B **25**, 1983 (1982).
[19]J. Callaway and C. S. Wang, Phys. Rev. B **16**, 2095 (1977).
[20]B. J. Jönsson-Akerman, R. Escudero, C. Leighton, S. Kim, I. K. Schuller, and D. A. Rabson, Appl. Phys. Lett. **77**, 1870 (2000).
[21]J. G. Simmons, J. Appl. Phys. **34**, 1793 (1963).
[22]J. Halbritter, Surf. Sci. **122**, 80 (1982).
[23]M. Jullière, Phys. Lett. **54A**, 225 (1975).
[24]R. Meservey and P. M. Tedrow, Phys. Rep. **238**, 173 (1994).
[25]J. Hermanson, Solid State Commun. **22**, 9 (1977).
[26]W. Eberhardt and F. J. Himpsel, Phys. Rev. B **21**, 5572 (1980).
[27]J. M. MacLaren, X.-G. Zhang, W. H. Butler, and X. Wang, Phys. Rev. B **59**, 5470 (1999).
[28]N. Daude, C. Jouanin, and C. Gout, Phys. Rev. B **15**, 2399 (1977).